

[Handwritten signature]

12 LEVEL II

ADL-TR-1917
August 1980

**Gigawatt Microwave Emission from a
Relativistic Reflex Triode**

by **Howard E. Brandt**
Alan Bromborsky
Henry B. Bruns
Richard A. Kehn
George P. Laska

DTIC
ELECTE
OCT 20 1980
S D
B

AD A090598



**U.S. Army Electronics Research
and Development Command**
Harry Diamond Laboratories
Adelphi, MD 20783

Approved for public release; distribution unlimited.

FILE COPY

80 10 15 008

The findings in this report are not to be construed as an official Department of the Army position unless so designated by other authorized documents.

Citation of manufacturer's or trade names does not constitute an official indorsement or approval of the use thereof.

Destroy this report when it is no longer needed. Do not return it to the originator.

A preliminary version of this report was issued as PRL-30-5 in January 1950.

UNCLASSIFIED

SECURITY CLASSIFICATION OF THIS PAGE (When Data Entered)

REPORT DOCUMENTATION PAGE		READ INSTRUCTIONS BEFORE COMPLETING FORM
14 1. REPORT NUMBER HDL-TR-1917	2. GOVT ACCESSION NO. AD-A090598	3. RECIPIENT'S CATALOG NUMBER
6 4. TITLE (and Subtitle) Gigawatt Microwave Emission from a Relativistic Reflex Triode.	9 5. TYPE OF REPORT & PERIOD COVERED Technical Report.	6. PERFORMING ORG. REPORT NUMBER
10 7. AUTHOR(s) Howard E./Brandt Richard A./Kehs Alan/Bromborsky George P./Lasche Henry B./Bruns	8. CONTRACT OR GRANT NUMBER(s)	
8. PERFORMING ORGANIZATION NAME AND ADDRESS Harry Diamond Laboratories 2800 Powder Mill Road Adelphi, MD 20783	10. PROGRAM ELEMENT, PROJECT, TASK AREA & WORK UNIT NUMBERS Program Ele: 6.11.01.A	
11. CONTROLLING OFFICE NAME AND ADDRESS US Army Materiel Development and Readiness Command Alexandria, VA 22333	11 11. REPORT DATE August 1980	13. NUMBER OF PAGES 27
14. MONITORING AGENCY NAME & ADDRESS (if different from Controlling Office)	15. SECURITY CLASS. (of this report) UNCLASSIFIED	15a. DECLASSIFICATION/DOWNGRADING SCHEDULE
12/26		
16. DISTRIBUTION STATEMENT (of this Report) Approved for public release; distribution unlimited.		
17. DISTRIBUTION STATEMENT (of the abstract entered in Block 20, if different from Report)		
16 18. SUPPLEMENTARY NOTES DRCMS Code: 51110191, A0011 DA Project: 1L161101A91A HDL Project: A10025		
19. KEY WORDS (Continue on reverse side if necessary and identify by block number) Microwave source Collective electron dynamics Reflex triode Space charge effects Relativistic electron beam Nonneutral plasmas Particle simulation		
20. ABSTRACT (Continue on reverse side if necessary and identify by block number) Single microwave bursts in X-band of 10-ns duration at gigawatt power levels have been obtained at the Harry Diamond Laboratories with the relativistic reflex triode. The associated relativistic space-charge oscillations have rich high-frequency content. The dominant radiated modes are determined by gap spacing, beam diameter, and gap voltage. The theory of the collective electron space-charge oscillations and the resultant microwave power spectrum is reviewed and compared with experiment.		

DD FORM 1 JAN 73 1473 EDITION OF 1 NOV 65 IS OBSOLETE

UNCLASSIFIED
SECURITY CLASSIFICATION OF THIS PAGE (When Data Entered)

1

163050

CONTENTS

	<u>Page</u>
1. INTRODUCTION.....	5
2. RELATIVISTIC REFLEX TRIODE.....	6
3. SHEET MODEL OF TRIODE DYNAMICS.....	7
4. ELECTRON SPACE-CHARGE DYNAMICS.....	13
5. MICROWAVE SPECTRUM.....	15
6. CONCLUSIONS.....	19
LITERATURE CITED.....	21
DISTRIBUTION.....	23

FIGURES

1 Reflex triode tank, FX-45 pulsed power source, and microwave diagnostics.....	7
2 Reflex triode attached to FX-45 pulse line.....	8
3 Triode model geometry.....	9
4 Sheet model.....	10
5 Space-charge density over one dominant cycle as function of distance from cathode for constant applied voltage of 1 MV.....	14
6 Extremal forms of potential function for constant applied voltage of 1 MV.....	15
7 Calculated average power spectrum for applied voltage ramp rising to 1 MV in 10 ns with 9.5-mm gap.....	17
8 Calculated average power spectrum for applied voltage ramp rising to 2 MV in 25 ns with 1-cm gap.....	18

S DTIC ELECTE **D**
 OCT 20 1980
B

3

Accession For	
NTIS GRA&I	<input checked="" type="checkbox"/>
DTIC TAB	<input type="checkbox"/>
Unannounced	<input type="checkbox"/>
Justification	
By	
Distribution/	
Availability Codes	
Dist	Avail and/or Special
A	

1. INTRODUCTION

Gigawatt microwave power levels in X-band have been obtained* at the Harry Diamond Laboratories by using a relativistic-electron-beam reflex triode.¹ In these experiments, explosive electron emission² from a carbon cathode delivered ~15 to 20 kA average current through the triode region in a 25-ns pulsed accelerating potential of 1 to 2 MV (peak). The grid, ~1 cm from the emission cathode, consisted of a 0.25-mil (6.35- μ m) aluminized Mylar foil. An external magnetic field directed along the triode axis was 0.1 to 0.4 Tesla. The associated relativistic space-charge oscillations³ had rich frequency content. The dominant modes were determined by gap spacing, gap voltage, and magnetic field. The polarization was primarily along the beam. Single microwave bursts of ~10 ns at gigawatt power levels were achieved. The conversion efficiency of electron beam power to microwave power was ~1 to 2 percent.

The theory of the collective electron space-charge oscillations in the reflex triode and the resultant microwave power spectrum and comparison with experiment were recently summarized in an oral presentation at the 21st Annual Meeting of the Division of Plasma Physics of the American Physical Society in Boston.⁴ This report documents that presentation.

In section 2, the reflex triode design is described. In section 3, the one-dimensional time-dependent relativistic sheet model of the triode dynamics is outlined. In section 4, the calculated space-charge oscillations, charge bunching, virtual cathode formation, and potential are discussed. In section 5, the calculated microwave spectrum is described; in section 6, several conclusions are presented.

¹H. E. Brandt, A. Bromborsky, H. B. Bruns, and R. A. Kehs, *Proc. 2nd International Topical Conference on High Power Electron and Ion Beam Research and Technology, II*, Cornell University (October 1977), 649.

²Robert K. Parker, *Explosive Electron Emission and the Characteristics of High-Current Electron Flow* (1974). (AD 775 992)

³H. E. Brandt and A. Bromborsky, *Bull. Am. Phys. Soc.*, 22 (1977), 1131.

⁴H. E. Brandt, A. Bromborsky, H. B. Bruns, R. A. Kehs, and G. Lasche, *Bull. Am. Phys. Soc.*, 24 (1979), 1077.

*A. Bromborsky, H. E. Brandt, H. B. Bruns, R. Kehs, and G. Lasche, *Presentation at 20th Annual Meeting of Division of Plasma Physics, Am. Phys. Soc.* (October 1978).

2. RELATIVISTIC REFLEX TRIODE

The relativistic reflex triode^{1,5} is a high-voltage electron tube with an electrode configuration analogous to that of the older and much smaller triode tube of conventional electronics. Figure 1 shows the tank containing the reflex triode connected to the FX-45 pulsed power source.^{6,7} The latter is a 60-ohm coaxial transmission line charged by a Van de Graaff generator and discharged via a triggered spark gap. The line is charged to a potential 3.0 MV, thereby storing 0.8 kJ of energy. The X-band and Ku-band microwave diagnostic waveguides also are seen in figure 1 facing the window of the triode tank. The reflex triode itself is located inside the tank as shown in figure 2. The anode (grid) consists of an 8-in. (20.3-cm)-diameter copper-plated fiberglass anode holder supporting a thin 6.35- μ m aluminized Mylar foil and is connected to the positive center conductor of the FX-45 pulse line. The carbon cathode is 5 cm in diameter, and the cathode-anode gap is 1 cm. The cathode-ground plane gap is 10.5 cm. The emission cathode is attached to the outer conductor of the pulse line, and both are at ground plane potential. A slow pulsed (\sim 300 Hz) axial magnetic field of peak amplitude 0.4 Tesla is applied along the cathode-anode axis in figure 2 (p. 8). Also shown in figure 2 are carbon activation targets for monitoring ion currents produced at the anode.

When the reflex triode is fired, a voltage pulse of \sim 1 MV moves down the pulse line and across the cathode-anode gap, explosively² pulling 15 to 20 kA of average current of electrons from the emission cathode. The physics of the explosive cathode emission is complex.² The triode region fills with a relativistic gas of electrons, which undergoes collective relativistic space-charge oscillations about the anode foil. These electron space-charge oscillations are naturally accompanied by intense radiative emissions transverse to the beam and polarized parallel to the beam.

¹H. E. Brandt, .. Bromborsky, H. B. Bruns, and R. A. Kehs, *Proc. 2nd International Topical Conference on High Power Electron and Ion Beam Research and Technology, II*, Cornell University (October 1977), 649.

²Robert K. Parker, *Explosive Electron Emission and the Characteristics of High-Current Electron Flow* (1974). (AD 775 992)

⁵S. Humphries, T. I. Lee, and R. N. Sudan, *Appl. Phys. Lett.*, 25 (1974), 20.

⁶Final Report: *Super Flash X-Ray System*, Ion Physics Corp., Burlington, MA, Contract DA-49-186-AMC-175(D) (1966).

⁷FX-45 Machine for Harry Diamond Laboratories Operation and Maintenance Manual, Ion Physics Corp., Burlington, MA, Contract DA-49-186-AMC-175(D) (1966).

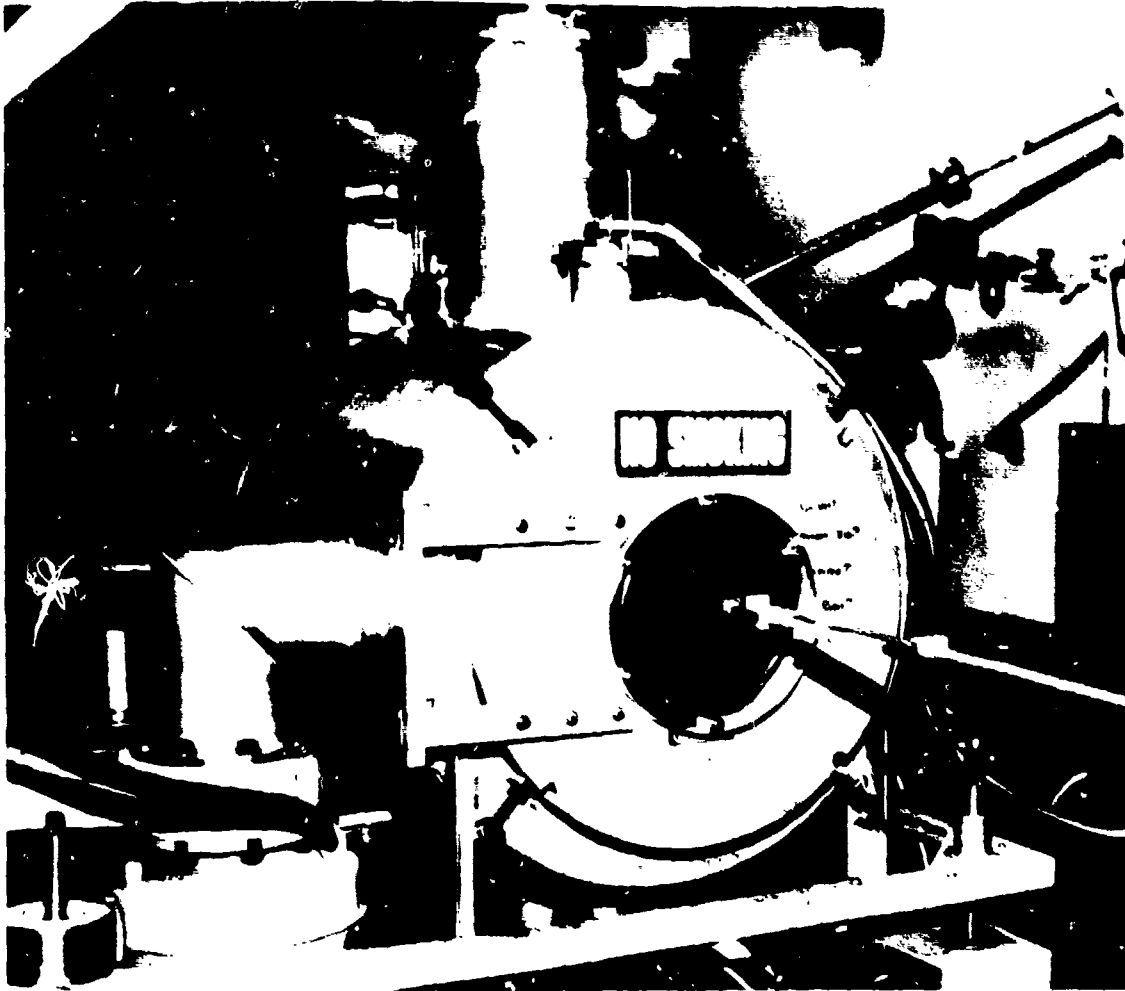


Figure 1. Reflex triode tank, FX-45 pulsed power source, and microwave diagnostics.

3. SHEET MODEL OF TRIODE DYNAMICS

To describe the essential underlying electron dynamics in the triode region, we approximate the real three-dimensional time-dependent configuration by the one-dimensional time-dependent configuration shown in figure 3. The primary motivation for a one-dimensional representation is minimization of computational cost. In support of this is the fact that the applied magnetic field confines the beam in the radial direction. In the limit of an extremely strong magnetic field, the electron motion would be confined to the magnetic field lines. Although

this extreme does not apply for the given experimental configuration, we assumed that the dominant force is that due to the high applied voltage so that, to first order, the electron motion is predominantly along the triode axis. Full determination of the importance of transverse effects awaits the completion of a simulation including the effects of transverse electric and magnetic fields due to electron space charge and currents. In the relativistic regime, magnetic field effects are often very important; however, the one-dimensional model precludes the inclusions of magnetic forces. One would expect the one-dimensional model to be best for the case of a very large ratio of cathode diameter to cathode-anode gap. In this case, ignoring magnetic field effects at least in the interior region of the discharge would be justified.



Figure 2. Reflex triode attached to FX-45 pulse line.

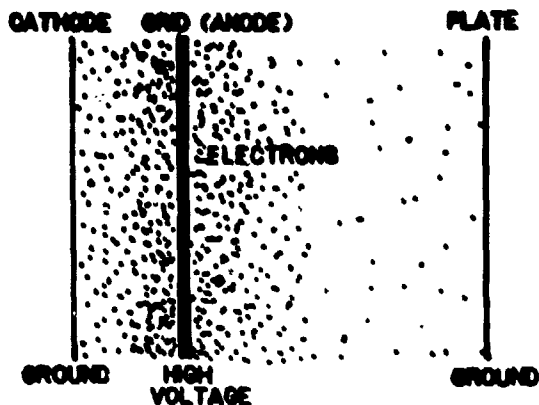


Figure 3. Triode model geometry.

In figure 3, the cathode and plate planes are taken to be at ground (zero) electrical potential. The anode plane is at the potential of the prescribed voltage pulse.

The next level of abstraction is to represent the relativistic electron gas within the triode region by a sheet representation as depicted in figure 4. Thus, the electron space-charge density, $\rho(x,t)$, at any instant, t , as a function of distance, x , from the emission cathode plane is represented by

$$\rho(x,t) = \lim_{M(t) \rightarrow \infty} \sigma_M \sum_{m=1}^{M(t)} \delta(x - x_m(t)) \quad (1)$$

Here, $M(t)$ is the number of sheets in the triode region at time t , σ_M is the charge density of each sheet and is taken to be the same for each sheet, δ is the one-dimensional Dirac delta function, and $x_m(t)$ is the position of the m th sheet at time t . In practice, the infinite limit in equation (1) must clearly be replaced by a finite one, which we take to be the time averaged number of sheets in the triode region. M should be chosen as large as simulation cost permits. The dynamics will control coordinates $x_m(t)$ and spacing of the constant and equal charge density sheets so that regions of high charge density will have a high density of sheets.

A primary theoretical weakness of the sheet model is that, in practice, each sheet will correspond to $\sim 10^{10}$ electrons, whose separate degrees of freedom are ignored and which are effectively constrained to move bound together as a whole. This same fundamental criticism holds also for particle in-cell models and, for that matter, for any "fluid element" representation. For the model at hand, this problem is less serious, the larger the choice of M . The final justification for the

sufficient largeness of M is the convergence of quantities of interest. However, in practice, establishing such convergence is prohibited by cost and the difficulty of even quasi-analytical proof.

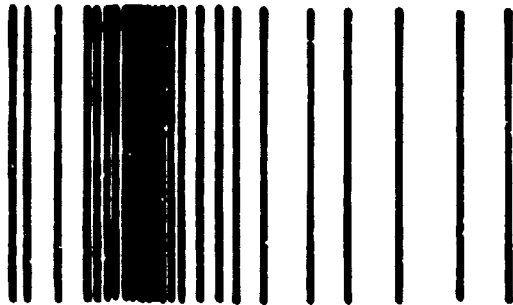


Figure 4. Sheet model.

In the simple model presented here, ion formation at the anode and the resulting ionic component of the charge distribution are ignored on the grounds that significant ion displacement will be relatively delayed because of the large ion-to-electron-mass ratio. It is the ion current that ultimately produces gap closure and limits the duration of the applied voltage pulse.

The electric field, $E(x_n, t)$, at location x_n of the n th sheet at time t , due to both the externally applied voltage, $V(t)$, and the space-charge fields arising from all the other sheets, is determined by solving Poisson's equation, which results in

$$E(x_n, t) = \begin{cases} \frac{\sigma}{\epsilon_0} \left\{ -[M_1(t) - M_{11}(x_n(t))] \right. \\ \quad \left. + \frac{1}{2} + M_1(t) \frac{\bar{x}_1(t)}{d_1} \right\} - \frac{V(t)}{d_1}, & 0 < x_n \leq d_1 \\ \frac{\sigma}{\epsilon_0} \left\{ -[M_2(t) - M_{21}(x_n(t))] \right. \\ \quad \left. + \frac{1}{2} + M_2(t) \frac{\bar{x}_2(t) - d_1}{d_2 - d_1} \right\} + \frac{V(t)}{d_2 - d_1}, & d_1 < x_n < d_2 \end{cases} \quad (2)$$

The upper expression holds at a sheet lying on the emission cathode side of the anode and the lower expression, on the plate side. Here d_1 is the cathode-anode gap, d_2 is the cathode-plate separation, σ is the sheet charge density, ϵ_0 is the permittivity of free space, $M_1(t)$ and $M_2(t)$ are the number of sheets on the cathode and plate sides of the anode, respectively, at time t , $M_{11}(x_n(t))$ is the number of sheets between the cathode and the n th sheet when it is on the cathode side of the anode, $M_{21}(x_n(t))$ is the number of sheets between the anode and the n th sheet when it is on the plate side, and $\bar{x}_1(t)$ and $\bar{x}_2(t)$ are the mean separations from the cathode for all sheets on the cathode and plate sides, respectively, of the anode.

The time step for the model is taken to be a small fraction of a cathode-anode light transit time. Since the electrons are limited by relativity to velocities less than the velocity of light, this choice of time step should provide sufficient time resolution of the electron dynamics. Thus, the time step, Δt , is given by

$$\Delta t = d_1 / Nc \quad (3)$$

where N is some large number and c is the speed of light.

Sheet electron momenta $p_n(t+\Delta t)$ and positions $x_n(t+\Delta t)$ at time $t + \Delta t$ are then easily expressed in terms of those at time t by use of the Lorentz force equation, by which one obtains

$$p_n(t+\Delta t) = p_n(t) + eE_n(t)\Delta t \quad , \quad (4)$$

$$x_n(t + \Delta t) = x_n(t) + \frac{1}{2} \left[1 + \left(\frac{p_n(t)}{mc} \right)^2 \right]^{-3/2} \times \left\{ \left[1 + 2 \left(\frac{p_n(t)}{mc} \right)^2 \right] \frac{p_n(t)}{mc} + \frac{p_n(t+\Delta t)}{mc} \right\} c\Delta t \quad . \quad (5)$$

Index n corresponds to the n th sheet, and e and m are the charge and the mass of the electron, respectively. A sheet is allowed to enter the triode region only at those time steps for which the total electric field points into the emission cathode. A sheet is taken to leave the system whenever it hits the plate or returns to the emission cathode. A sheet is also subtracted whenever the energy that it loses in passing through the anode foil reduces its kinetic energy to zero. Thus, the number of sheets, $M(t+\Delta t)$, at time $t + \Delta t$ is given in terms of the number of sheets at time t by

$$\begin{aligned}
N(t+\Delta t) &= N(t) + \Theta(-E(0,t)) \\
&- \sum_{m=1}^{M(t)} \left[\Theta(d_2 - x_m(t)) \Theta(x_m(t+\Delta t) - d_2) \right. \\
&+ \Theta(x_m(t)) \Theta(-x_m(t+\Delta t)) \\
&+ \Theta(d_1 - x_m(t)) \Theta(x_m(t+\Delta t) - d_1) \Theta(\Delta p_m - p_m(t+\Delta t)) \\
&\left. + \Theta(x_m(t) - d_1) \Theta(d_1 - x_m(t+\Delta t)) \Theta(\Delta p_m + p_m(t+\Delta t)) \right] .
\end{aligned} \tag{6}$$

Here, Θ is the theta function, $E(0,t)$ is the total electric field at the emission cathode, and Δp_m is the momentum loss experienced by the m th sheet in passing through the anode foil as determined by ionization and radiative loss tables.

The surface charge density, σ , of the sheets is determined by the following considerations. The triode charge in the triode region will build up to the point where it can contain no more; namely, further injection of charge will result in charge ejection. Under such a condition of space-charge saturation, we have shown³ that, in the parameter regime of interest, the total time averaged charge, \bar{Q} , in the triode region is proportional to the applied voltage, V , namely,

$$\bar{Q} = KV \quad . \tag{7}$$

We call the constant of proportionality, K , the space-charge capacity of the triode. It is independent of applied voltage and is determined only by the triode geometry.

The time averaged charge may be expressed in terms of the time averaged number of sheets, \bar{N} , by

$$\bar{Q} = A\sigma\bar{N} \quad , \tag{8}$$

where A is the cross-sectional area of the beam, which is assumed equal to the cathode area, and σ is the sheet surface charge density. By combining equations (7) and (8), the required sheet surface charge density is given by

$$\sigma = \frac{KV}{A\bar{N}} \quad . \tag{9}$$

³H. E. Brandt and A. Bromborsky, *Bull. Am. Phys. Soc.*, 22 (1977), 1131.

Therefore, in practice one chooses the averaged number of sheets to be some large, but affordable number to faithfully represent the space-charge distribution; the space-charge capacity is self-consistently calculated under conditions of space-charge saturation; the voltage and the beam area are given; and the sheet surface charge density is thereby determined.

Equations (1) to (9) form the algebraic basis for the numerical simulation. A FORTRAN program has been written whose present run cost is between \$30 and \$100 on the IBM System 370 computer. A typical set of program parameters in the experimental regime of current interest is $d_1 = 1$ cm and $N = 120$, resulting in 0.3-ps time resolution; $K = 8$ pF; a voltage ramp, $V(t)$, rises to $V = 2$ MV in 25 ns and then falls off linearly in 10 ns; $\bar{M} = 300$ sheets; $d_2 = 10.5$ cm; and $A = 20$ cm². In the following sections, the results of such simulations are discussed.

4. ELECTRON SPACE-CHARGE DYNAMICS

Numerical simulations based on the dynamical model presented in the preceding section reveal several significant characteristics of the relativistic electron space-charge dynamics in the triode. At the onset of the voltage pulse across the cathode-anode gap, electrons are explosively pulled out of the cathode plasma and fill up the triode region. The total space charge, however, is not monotonically increasing, but oscillates in time while rising to a saturated time averaged total charge. Electrons entering the gap with favorable phases relative to a given frequency component of the resultant space-charge fields give up energy to the fields and remain in the triode region, while those with unfavorable phases gain energy from the fields and are ejected from the triode region. Favorably phased electrons tend to be grouped together spatially since they enter about the same time. Also, space-charge limiting periodically limits the subsequent entrance of electrons at the emission cathode. These mechanisms give rise to electron space-charge bunching. While the electron bunches oscillate back and forth about the anode, they also interact with one another, ejecting and capturing electrons from one another and thereby being depleted and growing in size. Bunches are born and bunches die. This is the regime of strong Langmuir-like turbulence of the relativistic electron plasma.

Once the triode is saturated, the total charge oscillates about the mean saturated value. A fluctuating virtual cathode forms on the plate side of the anode at a time averaged distance approximately equal to the cathode-anode gap. Figure 5 displays a characteristic partial time evolution of the electron space-charge distribution in the triode region. This case is for a cathode-anode gap of 1 cm, a beam area of 20 cm², and a constant applied voltage of 1 MV. The plot covers a 100-ps time span that is 564 ps into the applied voltage pulse. This time span

was chosen to correspond to the period associated with the dominant spectral component of the space-charge oscillations, which in this case is 10 GHz. The spatial axis has its origin at the emission cathode, 1 cm down this axis is the anode plane, and the plate is beyond the plot at 10.5 cm. The electrons are concentrated within ~ 2 cm from the emission cathode with highest concentration just beyond the anode plane on the plate side. Transient bunching is evident with effective high-frequency sloshing about the anode. Spectral analysis of these space-charge oscillations reveals a broad spectrum of peaks in the gigahertz regime separated by ~ 0.2 to 0.4 GHz and peaking at 10 GHz. The location of the virtual cathode, which is characterized by a strong depletion of the charge density, is about 2 cm from the cathode and undergoes high-frequency oscillations. Thus at 564 ps and 664 ps, it is at ~ 2.5 cm, and at 614 ps it is at ~ 1.7 cm. For this example, at least, its position oscillates at the dominant frequency of ~ 10 GHz. One would expect a frequency of this order of magnitude to dominate, based on qualitative geometric considerations of near light velocity periodic transits of the 1-cm gap. Also of note is that small bunches of electrons do exist beyond the virtual cathode on the plate side. In fact, periodically some of these bunches hit the plate and are thereby ejected from the system.

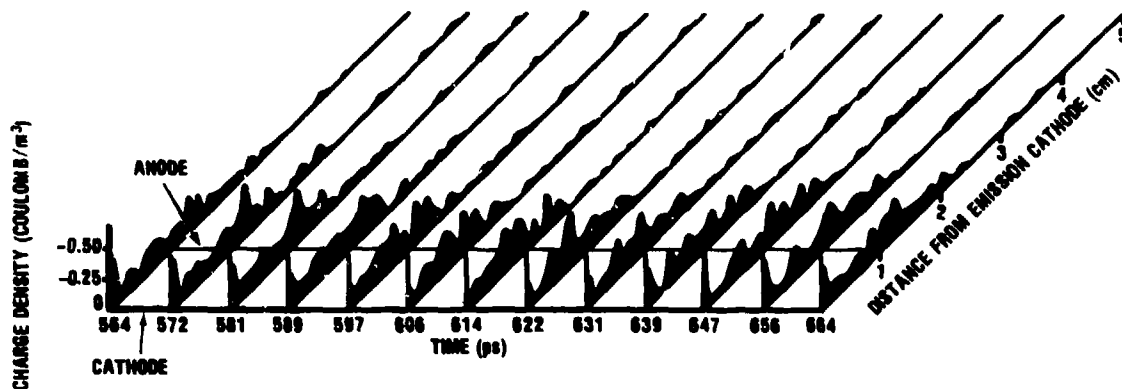


Figure 5. Space-charge density over one dominant cycle as function of distance from cathode for constant applied voltage of 1 MV.

The characterization of the virtual cathode dynamics is more evident in figure 6, which plots the total electrical potential during extremals of the virtual cathode position in figure 5 corresponding to a half cycle displacement. The location of the virtual cathode is characterized by a near discontinuity in the slope of the potential with a near linear spatial dependence on the plate side. The latter is to be ex-

pected on the basis of Poisson's equation and the approximately vanishing charge density on the plate side of the virtual cathode. Also of note is that the electrical potential at the virtual cathode is large. This feature is unique to the inherently time-dependent dynamics. Both the position and the potential of the virtual cathode undergo high-frequency oscillations.

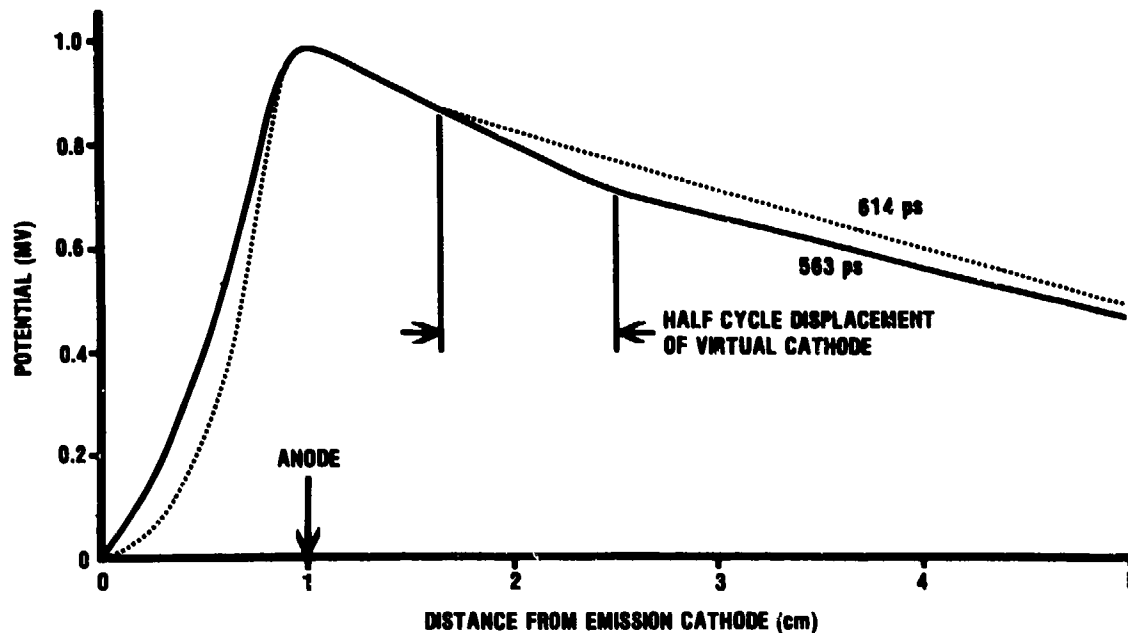


Figure 6. Extremal forms of potential function for constant applied voltage of 1 MV.

One would expect the high-frequency oscillations of the transient space-charge bunches in the triode region to radiate coherently like a superposition of dipole oscillators with polarization parallel to the beam. In the next section, the resultant calculated microwave power spectrum is discussed.

5. MICROWAVE SPECTRUM

It is assumed here that the real three-dimensional beam dynamics may be approximated by the one-dimensional model. For the cylindrical beam of radius R , the average power spectral density per steradian, $\langle d^2 P_{\perp} / d\omega d\Omega \rangle$, radiated perpendicular to the beam can be shown to be given by

$$\left\langle \frac{d^2 P_{\perp}}{d\omega d\Omega} \right\rangle = \frac{\mu_0 \pi \sigma^2 R^4}{4cT} \omega^2 |\Sigma(\omega)|^2 F^2(\omega) \quad (10)$$

where

$$\Sigma(\omega) = \frac{1}{2\pi} \int_{-\infty}^{\infty} dt e^{-i\omega t} \sum_{m=1}^{M(t)} v_m(t) \quad (11)$$

and

$$F(\omega) = \frac{2J_1\left(\frac{\omega R}{c}\right)}{\frac{\omega R}{c}} \quad (12)$$

Here, $d\Omega$ is the differential solid angle, μ_0 is the permeability of free space, σ is the sheet surface charge density, R is the beam radius, c is the speed of light, T is the voltage pulse duration, ω is the angular frequency, $M(t)$ is the number of sheets at time t , $v_m(t)$ is the velocity of the m th sheet at time t , and J_1 is the first order Bessel function of the first kind. Equation (10) is obtained by solving the wave equation with a current distribution represented by the calculated sheet dynamics, including radiative time delays only perpendicular to the beam, and by using the ordinary dipole far field approximation. The quantity $\Sigma(\omega)$ is the time Fourier transform of the sum of the sheet velocities. The quantity $F(\omega)$ is a geometric interference form factor resulting from the relative radiative time delays across the beam cross section. Computations of the power spectrum for an applied voltage ramp rising to 1 MV in 10 ns with a 9.5-mm gap are shown in figure 7. Those for 2 MV in 25 ns and a 1-cm gap are shown in figure 8. Plotted is the average transverse power spectral density as a function of frequency. The dips in the spectra around 7, 13, and 19 GHz, etc., are caused by the interference form factor, equation (12); namely, at those frequencies, $F(\omega)$ is vanishing and one has destructive interference. Aside from the modulation due to the interference form factor, the overall spectrum is broad with a high density of narrow spectral peaks separated by ~ 0.2 to 0.4 GHz. These multitudinous peaks are associated with the many mechanical modes of electron oscillation discussed in section 4.

However, the most intense spectral peak is at ~ 10 GHz in X-band, and it is fortuitous that the interference form factor also peaks there. This peak corresponds to the dominant mode of electron space-charge oscillation and also to that of the virtual cathode motion as discussed in section 4. Intense microwave emission also occurs in the L-, S-, C-, Ku-, and K-bands of the spectrum.

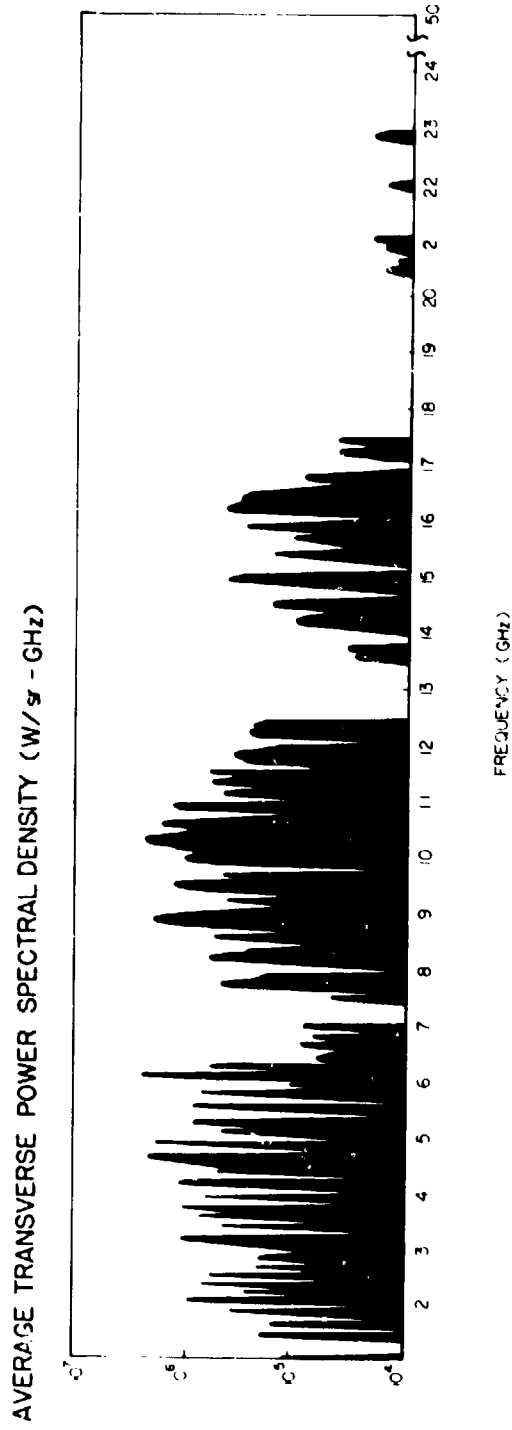


Figure 7. Calculated average power spectrum for applied voltage ramp rising to 1 MV in 10 ns with 9.5-mm gap.

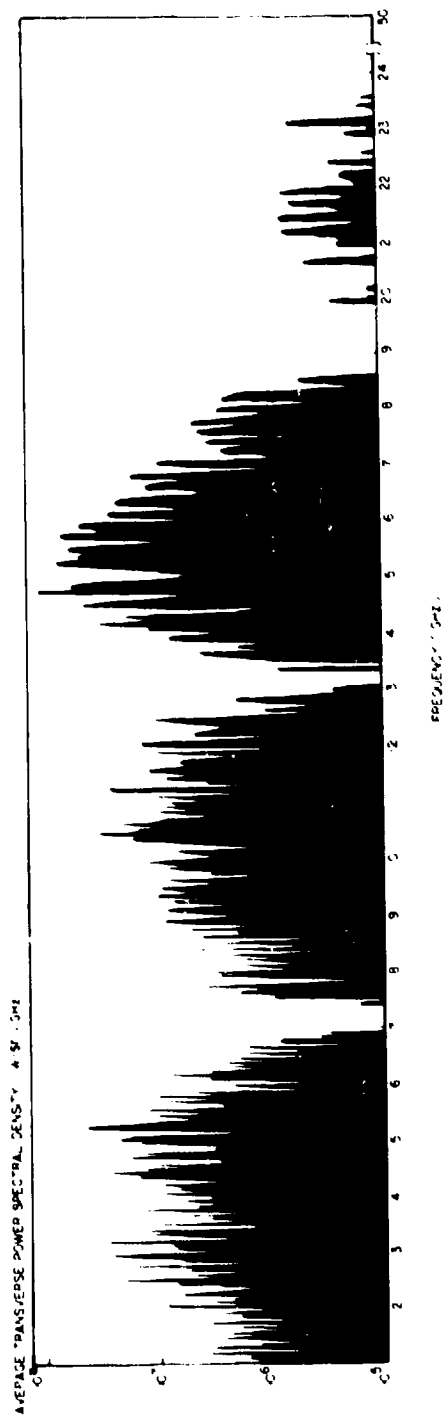


Figure 8. Calculated average power spectrum for applied voltage ramp rising to 2 MV in 25 ns with 1-cm gap.

Comparisons of these calculated microwave spectra with experiment show close agreement between calculated and observed frequencies and agreement to within a factor of two in average power. Thus, in recent experiments^{4,*} at the Harry Diamond Laboratories, average power levels of ~0.1 GW and peak power levels of ~1 GW centered in X-band at ~10 GHz were observed. Intense emissions in S-, Ku-, and K-bands also were observed. Experimental uncertainties in the voltage, current, and microwave measurements further underline the near agreement with the model calculations. Of particular importance is that the observed microwaves are dominantly polarized parallel to the electron beam; such polarization lends additional credence to the one-dimensional model.

The conversion efficiency of electron beam to X-band microwave power was only ~2 percent. However, this low efficiency does not indicate any fundamental limitation and most likely results from the poor impedance match between the triode (~6 ohms) and the FX-45 (~60 ohms). Of note is that 30-percent efficiency at gigawatt power levels in S-band has been achieved with a triode at the Tomsk Polytechnical Institute in the Soviet Union.⁸ The higher efficiency is likely due to the lower frequencies involved, the use of a resonant structure, and a good machine-triode impedance match. Earlier related microwave production experiments with a reflex triode at the Naval Research Laboratory resulted in 1.5-percent efficiency in X-band at 100-MW power levels.⁹

6. CONCLUSIONS

The relativistic one-dimensional time-dependent sheet model of the electron space-charge dynamics in the reflex triode reveals the occurrence of extensive transient space-charge bunching, a broad spectrum of multigigahertz frequency space-charge oscillations about the anode, and formation and high-frequency oscillation of a virtual cathode. Calculations of the resultant microwave spectra reveal broad band intense microwave production centered in X-band and consistent with experimental observation.

⁴H. E. Brandt, A. Bromborsky, H. B. Bruns, R. A. Kehs, and G. Lasche, *Bull. Am. Phys. Soc.*, 24 (1979), 1077.

⁸A. N. Didenko, Y. Y. Krasik, S. F. Pereygin, and G. P. Fomenko, *Pis'ma Zh. Tekhnicheskoy Fiz.*, 5 (1979), 321-325.

⁹R. A. Mahaffey, P. Sprangle, J. Golden, and S. A. Kapetanacos, *Phys. Rev. Lett.*, 39 (1977), 843.

*A. Bromborsky, H. E. Brandt, H. B. Bruns, R. Kehs, and G. Lasche, *Presentation at 20th Annual Meeting of Division of Plasma Physics, Am. Phys. Soc. (October 1978).*

Although the model ignores possible important three-dimensional effects--in particular, those due to magnetic fields--and employs a coarse grained sheet model representation, it does successfully characterize the main features of the radiated microwave spectrum. In particular, the model explains the occurrence of near gigawatt microwave power levels in X-band with polarization parallel to the beam.

It should be emphasized, however, that the one-dimensional model precludes parametric analyses of the effects of applied and induced magnetic fields. Recent experiments at the Harry Diamond Laboratories reveal a sensitive dependence of microwave production on the applied magnetic field.^{10,11,*} The fundamental theoretical problem of sheet dynamics as a representation of autonomous electron motion also should be kept in mind, especially as it might bear on very-high-frequency or low-wavelength phenomena.

Of special importance is the fact that gigawatt power levels are obtainable in the reflex triode without the aid of resonators. It is likely that tens of gigawatts could be obtained by careful resonator design. Special problems arising from the requirement of high voltage breakdown avoidance between the electrodes and the resonators must be solved. Also, the presence of a resonator will significantly alter the spectral distribution of the space-charge oscillations, and therefore the one-dimensional model will be inadequate for resonator design.

¹⁰G. P. Lasche, A. Bromborsky, R. Kehs, M. Litz, and H. E. Brandt, *Bull. Am. Phys. Soc.*, 24 (1979), 1070.

¹¹R. A. Kehs, H. E. Brandt, A. Bromborsky, and G. Lasche, *The Generation of Gigawatt Power Levels of Microwave Radiation, Army Science Conference, United States Military Academy, West Point, NY (1980)*.

*A. Bromborsky, H. E. Brandt, H. B. Bruns, R. Kehs, and G. Lasche, *Presentation at 20th Annual Meeting of Division of Plasma Physics, Am. Phys. Soc. (October 1978)*.

LITERATURE CITED

- (1) H. E. Brandt, A. Bromborsky, H. B. Bruns, and R. A. Kehs, Proc. 2nd International Topical Conference on High Power Electron and Ion Beam Research and Technology, II, Cornell University (October 1977), 649.
- (2) Robert K. Parker, Explosive Electron Emission and the Characteristics of High-Current Electron Flow (1974). (AD 775 992)
- (3) H. E. Brandt and A. Bromborsky, Bull. Am. Phys. Soc., 22 (1977), 1131.
- (4) H. E. Brandt, A. Bromborsky, H. B. Bruns, R. A. Kehs, and G. Lasche, Bull. Am. Phys. Soc., 24 (1979), 1077.
- (5) S. Humphries, T. I. Lee, and R. N. Sudan, Appl. Phys. Lett., 25 (1974), 20.
- (6) Final Report: Super Flash X-Ray System, Ion Physics Corp., Burlington, MA, Contract DA-49-186-AMC-175(D) (1966).
- (7) FX-45 Machine for Harry Diamond Laboratories Operation and Maintenance Manual, Ion Physics Corp., Burlington, MA, Contract DA-49-186-AMC-175(D) (1966).
- (8) A. N. Didenko, Y. Y. Krasik, S. F. Pereygin, and G. P. Fomenko, Pis'ma Zh. Tekhnicheskoy Fiz., 5 (1979), 321-325.
- (9) R. A. Mahaffey, P. Sprangle, J. Golden, and S. A. Kapetanacos, Phys. Rev. Lett., 39 (1977), 843.
- (10) G. P. Lasche, A. Bromborsky, R. Kehs, M. Litz, and H. E. Brandt, Bull. Am. Phys. Soc., 24 (1979), 1070.
- (11) R. A. Kehs, H. E. Brandt, A. Bromborsky, and G. Lasche, The Generation of Gigawatt Power Levels of Microwave Radiation, Army Science Conference, United States Military Academy, West Point, NY (1980).

DISTRIBUTION

ADMINISTRATOR
DEFENSE DOCUMENTATION CENTER
ATTN DDC-TCA (12 COPIES)
CAMERON STATION, BUILDING 5
ALEXANDRIA, VA 22314

COMMANDER
US ARMY RSCH & STD GP (EUR)
ATTN LTC JAMES M. KENNEDY, JR.
CHIEF, PHYSICS & MATH BRANCH
FPO NEW YORK 09510

COMMANDER
US ARMY ARMAMENT MATERIEL
READINESS COMMAND
ATTN DR SAR-LEP-L, TECHNICAL LIBRARY
ROCK ISLAND, IL 61299

COMMANDER
US ARMY MISSILE & MUNITIONS
CENTER & SCHOOL
ATTN ATSK-CTD-F
REDSTONE ARSENAL, AL 35809

DIRECTOR
US ARMY MATERIEL SYSTEMS
ANALYSIS ACTIVITY
ATTN DR XSY-MP
ABERDEEN PROVING GROUND, MD 21005

DIRECTOR
US ARMY BALLISTIC RESEARCH LABORATORY
ATTN DR DAR-TSB-G (STINFO)
ATTN D. ECCLESHELL
ABERDEEN PROVING GROUND, MD 21005

TELEDYNE BROWN ENGINEERING
CUMMINGS RESEARCH PARK
ATTN DR. MELVIN L. PRICE, MS-44
HUNTSVILLE, AL 35807

ENGINEERING SOCIETIES LIBRARY
345 EAST 47TH STREET
ATTN ACQUISITIONS DEPARTMENT
NEW YORK, NY 10017

WRIGHT PATTERSON AFB
FOREIGN TECHNOLOGY DIVISION/FTD
ATTN J. BUTLER
WRIGHT PATTERSON AFB, OH 45433

US ARMY ELECTRONICS TECHNOLOGY
& DEVICES LABORATORY
ATTN DELET-DD
ATTN N. WILSON
FORT MONMOUTH, NJ 07703

OFFICE OF SECRETARY OF DEFENSE
ATTN ANTHONY J. TETHER
RM 3C2C0, THE PENTAGON
WASHINGTON, DC 20301

UNDER SECRETARY OF DEFENSE
FOR RESEARCH & ENGINEERING
ATTN DEP DIR (RESEARCH &
ADVANCED TECH)
WASHINGTON, DC 20301

CENTRAL INTELLIGENCE AGENCY
ATTN R. PETTIS
P.O. BOX 1925
WASHINGTON, DC 20013

US ARMY ERADCOM
ATTN C. M. DESANTIS
FORT MONMOUTH, NJ 07753

DEPARTMENT OF ENERGY
ATTN T. F. GODLOVE
ATTN M. MURPHY
ATTN A. COLE
WASHINGTON, DC 20595

BROOKHAVEN NATIONAL LABORATORY
ASSOCIATED UNIVERSITIES, INC.
ATTN PHYSICS DEPT
UPTON, LONG ISLAND, NY 11973

AMES LABORATORY (ERDA)
IOWA STATE UNIVERSITY
ATTN NUCLEAR SCIENCE CATEGORY
AMES, IA 50011

DEPARTMENT OF COMMERCE
NATIONAL BUREAU OF STANDARDS
ATTN LIBRARY
WASHINGTON, DC 20234

DEPARTMENT OF COMMERCE
NATIONAL BUREAU OF STANDARDS
CENTER FOR RADIATION RESEARCH
WASHINGTON, DC 20234

NATIONAL BUREAU OF STANDARDS
ATTN J. WAIT
BOULDER, CO 80303

US ENERGY RESEARCH & DEVELOPMENT
ADMINISTRATION
ATTN 1ST ADMIN FOR NUCLEAR ENERGY
ATTN OFFICE OF TECHNICAL INFORMATICS
WASHINGTON, DC 20545

DIRECTOR
DEFENSE ADVANCED RESEARCH
PROJECTS AGENCY
ATTN D. H. TANIMOTO
ATTN A. PIKE
ATTN J. MANGANO
ATTN J. R. BAYLESS
ARCHITECT BLDG
1400 WILSON BLVD
ARLINGTON, VA 22209

DISTRIBUTION (Cont'd)

DIRECTOR
DEFENSE COMMUNICATIONS AGENCY
WASHINGTON, DC 20305

DIRECTOR
DEFENSE INTELLIGENCE AGENCY
ATTN DT-1, NUCLEAR & APPLIED
SCIENCES DIV
ATTN ELECTRONIC WARFARE BRANCH
ATTN M. L. AITEL
WASHINGTON, DC 20301

CHIEF
LIVERMORE DIVISION, FIELD COMMAND, DNA
LAWRENCE LIVERMORE LABORATORY
P.O. BOX 808
LIVERMORE, CA 94550

DIRECTOR
NATIONAL SECURITY AGENCY
ATTN TECHNICAL LIBRARY
ATTN F. REDARD
FORT GEORGE G. MEADE, MD 20755

DIRECTOR
DEFENSE NUCLEAR AGENCY
ATTN E. E. CONRAD, DEP DIR,
SCIENTIFIC TECHNOLOGY
ATTN RAEV, ELECTRONIC VULNERABILITY
ATTN R. OSWALD
ATTN P. GULLICKSON
WASHINGTON, DC 20305

DEFENSE RESEARCH AND ENGINEERING
DIRECTED ENERGY TECHNOLOGY OFFICE
ATTN G. GAMOTA
ATTN J. R. AIREY
THE PENTAGON
WASHINGTON, DC 20301

ASSISTANT SECRETARY OF THE ARMY (R&D)
ATTN DEP FOR SCI & TECH
WASHINGTON, DC 20310

OFFICE, DEPUTY CHIEF OF STAFF
FOR OPERATIONS & PLANS
DEPT OF THE ARMY
ATTN DAMO-SSN, NUCLEAR DIV
WASHINGTON, DC 20310

OFFICE OF THE DUPTY CHIEF OF STAFF
FOR RESEARCH, DEVELOPMENT,
& ACQUISITION
DEPART OF THE ARMY
ATTN DAMA-ARZ-A, CHIEF SCIENTIST,
DA & DIRECTOR OF ARMY RESEARCH,
M. E. LASSER
ATTN DAMA-CSS-N, NUCLEAR TEAM
ATTN F. D. VERDERAME
WASHINGTON, DC 20310

COMMANDER
BALLISTIC MISSILE DEFENSE
ADVANCED TECHNOLOGY CENTER
ATTN D. SCHENK
P.O. BOX 1500
HUNTSVILLE, AL 35807

COMMANDER
US ARMY FOREIGN SCIENCE
& TECHNOLOGY CENTER
FEDERAL OFFICE BLDG
ATTN DRXST-SD, SCIENCES DIV
ATTN T. CALDWELL
220 7TH STREET, NE
CHARLOTTESVILLE, VA 22901

COMMANDER
US ARMY MATERIALS & MECHANICS
RESEARCH CENTER
ATTN DRXMR-H, BALLISTIC MISSILE
DEF MATLS PROG OFC
WATERTOWN, MA 02172

COMMANDER
US ARMY MISSILE COMMAND
ATTN DRDMI-TR, PHYSICAL SCIENCES DIR
REDSTONE ARSENAL, AL 35809

ARMY RESEARCH OFFICE (DURHAM)
P.O. BOX 12211
ATTN H. ROBL
ATTN R. LONTZ
ATTN B. D. GUENTHER
ATTN TECH LIBRARY
ATTN F. DELUCCIA
RESEARCH TRIANGLE PARK, NC 27709

COMMANDER
US ARMY ABERDEEN PROVING GROUND
ATTN STEAP-TL, TECH LIB
ABERDEEN PROVING GROUND, MD 21005

NAVAL AIR SYSTEMS COMMAND
ATTN R. J. WASNESKI
WASHINGTON, DC 20361

SUPERINTENDANT
NAVAL POSTGRADUATE SCHOOL
ATTN LIBRARY, CODE 2124
MONTEREY, CA 93940

DIRECTOR
NAVAL RESEARCH LABORATORY
ATTN 2600, TECHNICAL INFO DIV
ATTN 5540, LASER PHYSICS
ATTN 6000, MATL & RADIATION SCI & TE
ATTN B. RIPIN
ATTN L. A. COSBY
ATTN E. E. KEMPE
ATTN J. T. SCHRIEMPF
ATTN R. F. WENZEL

DISTRIBUTION (Cont'd)

NAVAL RESEARCH LABORATORY (Cont'd)

ATTN R. HETTCHE
ATTN J. GOLDEN
ATTN V. L. GRANATSTEIN
ATTN R. K. PARKER
ATTN P. A. SPRINGLE
ATTN C. A. KAPETANAKAS
ATTN S. AHN
ATTN T. P. COFFEY
WASHINGTON, DC 20375

COMMANDER
NAVAL SURFACE WEAPONS CENTER
ATTN V. PUGLIELLI
ATTN DX-21, LIBRARY DIV
DAHLGREN, VA 22448

OFFICE OF NAVAL RESEARCH
ATTN W. J. CONDELL
800 N. QUINCY ST
ARLINGTON, VA 22217

COMMANDER
NAVAL SURFACE WEAPONS CENTER
ATTN H. UHM
ATTN WA-13, HIGH-ENERGY LASER BR
ATTN WA-50, NUCLEAR WEAPONS
EFFECTS DIV
ATTN WR, RESEARCH & TECHNOLOGY DEPT
ATTN WR-40, RADIATION DIV
ATTN WX-40, TECHNICAL LIB
WHITE OAK, MD 20910

NAVAL MATERIAL COMMAND
ATTN T. HORWATH
2211 JEFFERSON DAVIS HWY
WASHINGTON, DC 20301

COMMANDER
NAVAL WEAPONS CENTER
ATTN 315, LASER/INFRARED SYS DIV
ATTN 381, PHYSICS DIV
CHINA LAKE, CA 93555

NAVAL INTELLIGENCE SUPPORT CENTER
ATTN M. KOONTZ
4301 SUITLAND RD.
SUITLAND, MD 20390

DAVID TAYLOR MODEL BASIN
ATTN G. MAIDANIK
BETHESDA, MD 20084

PATRICK AFB
ATTN T. E. MAULTSBY
PATRICK AFB, FL 32931

ASSISTANT SECRETARY OF THE AIR FORCE
(RESEARCH & DEVELOPMENT)
WASHINGTON, DC 20330

DIRECTOR
AF OFFICE OF SCIENTIFIC RESEARCH
BOLLING AFB
ATTN NP, DIR OF PHYSICS
ATTN R. BARKER
WASHINGTON, DC 20332

COMMANDER
AF WEAPONS LAB, AFSC
ATTN D. J. SULLIVAN
ATTN M. L. ALME
ATTN A. H. GUENTHER
ATTN W. E. PAGE
ATTN D SULLIVAN
ATTN LR, LASER DEV DIV
KIRTLAND AFB, NM 87117

ADMINISTRATOR
NASA HEADQUARTERS
WASHINGTON, DC 20546

AMES RESEARCH CENTER
NASA
ATTN TECHNICAL INFO DIV
MOFFETT FIELD, CA 94035

DIRECTOR
NASA
GODDARD SPACE FLIGHT CENTER
ATTN 250, TECH INFO DIV
GREENBELT, MD 20771

OAK RIDGE NATIONAL LABORATORY
P.O. BOX Y
ATTN A. C. ENGLAND
OAK RIDGE, TN 37830

NATIONAL RESEARCH COUNCIL
DIVISION OF PHYSICS
ATTN P. JAANIMAGI
OTTAWA, ONTARIO
CANADA

INSTITUTE OF EXPERIMENTAL PHYSIK V
RUHR-UNIVERSITY
POSTFACH 2148
ATTN H. KUNZE
436 BOCHUM, WEST GERMANY

PHYSICS INTERNATIONAL
2700 MERCER ST
ATTN B. A. LIPPMANN
ATTN R. D. GENUARIO
SAN LEANDRO, CA 94577

SRI INTERNATIONAL
ATTN G. AUGUST
ATTN C. L. RINO
333 RAVENSWOOD AVE
MENLO PARK, CA 94025

DISTRIBUTION (Cont'd)

B. K. DYNAMICS
ATTN J. M. RAIPAN
ATTN R. J. LINE
ATTN I. F. KUHN, JR.
ATTN A. W. FLIFLET
15825 SHADY GROVE RD
ROCKVILLE, MD 20850

FUSION ASSOC
ATTN D. L. ENSLEY
P O BOX 1274
EUREKA, CA 95501

GENERAL DYNAMICS CORP
ATTN H. T. BUSCHER
POMONA DIVISION
P.O. BOX 2507
POMONA, CA 91766

GENERAL ELECTRIC CO.
ATTN J. W. QUINE
PO BOX 1072
SCHENECTADY, NY 12345

R. C. HANSEN, INC.
ATTN R. C. HANSEN
BOX 215
TARZANA, CA 91356

JAYCOR
ATTN R. A. MAHAFFEY
205 S. WHITING ST
ALEXANDRIA, VA 22304

LAWRENCE LIVERMORE LABORATORY
UNIVERSITY OF CALIFORNIA
ATTN V. W. SLIVINSKY
ATTN S. L. YU
ATTN G. CRAIG
ATTN J. WYATT
ATTN R. ALVAREZ
ATTN G. LASCHE (10 COPIES)
PO BOX 808
LIVERMORE, CA 94550

LOCKHEED MISSILE & SPACE CO
ATTN A. D. MACDONALD
3056 GREER RD
PALO ALTO, CA 94303

LOS ALAMOS SCI LAB
ATTN D. FORSLAND
ATTN C. M. FOWLER
ATTN B. WARNER
ATTN J. LANDT
ATTN T. R. KING
ATTN R. W. FREYMAN
ATTN A. W. CHURMATZ
ATTN L. M. DUNCAN
P.O. BOX 1663
LOS ALAMOS, NM 87545

MAXWELL LABORATORIES
ATTN J. S. PEARLMAN
8835 BALBOA AVE
SAN DIEGO, CA 92123

PHYSICAL SCIENCE, INC.
ATTN R. WEISS
ATTN E. PUGH
30 COMMERCE WAY
WOBURN, MA 01801

R&D ASSOCIATES
ATTN R. LELEVIER
ATTN E. MARTINELLI
ATTN W. R. GRAHAM
P.O. BOX 9695
MARINA DEL REY, CA 90291

THE RAND CORPORATION
ATTN S. KASSEL
2100 M ST NW
WASHINGTON, DC 20037

SANDIA LABORATORIES
ATTN S. HUMPHRIES, JR.
ATTN E. F. HARTMAN
ATTN F. COPPAGE
4244 SANDIA LABS
ALBUQUERQUE, NM 87115

W. J. SCHAFER ASSOC
ATTN J. P. REILLY
10 LAKESIDE OFFICE PARK
WAKEFIELD, MA 01880

SCIENCE APPLICATIONS INC
ATTN F. CHILTON
1200 PROSPECT ST
P.O. BOX 2351
LA JOLLA, CA 92038

TRW
ATTN D. ARNUSH
ONE SPACE PARK
REDONDO BEACH, CA 90278

WESTERN RESEARCH CORP
ATTN R. O. HUNTER
225 BROADWAY, SUITE 1600
SAN DIEGO, CA 92101

CALIFORNIA INSTITUTE OF TECHNOLOGY
ATTN J. MERCEREAU
PASADENA, CA 91125

UNIVERSITY OF CALIFORNIA
PHYSICS DEPT
ATTN K. WATSON
BERKELEY, CA 94720

UNIVERSITY OF CALIFORNIA
ELECTRICAL ENGINEERING DEPT
ATTN C. K. BIRDSALL
BERKELEY, CA 94720

DISTRIBUTION (Cont'd)

UNIVERSITY OF CALIFORNIA, DAVIS
APPLIED SCIENCES
ATTN J. DEGROOT
DAVIS, CA 95616

UNIVERSITY OF CALIFORNIA SAN DIEGO
PHYSICS DEPT
ATTN N. KROLL
LA JOLLA, CA 92093

UNIVERSITY OF CALIFORNIA IRVINE
DEPT OF PHYSICS
ATTN G. BENFORD
ATTN N. ROSTOKER
IRVINE, CA 92717

CORNELL UNIVERSITY
ATTN R. N. SUDAN
ATTN, J. NATION
ATTN D. HAMMER
ITHACA, NY 14853

DARTMOUTH COLLEGE
PHYSICS DEPT
ATTN J. E. WALSH
HANOVER, NH 03755

UNIVERSITY OF MARYLAND
DEPT OF ELECTRICAL ENGINEERING
ATTN M. REISER
ATTN W. DESTLER
ATTN M. T. RHEE
COLLEGE PARK, MD 20742

UNIVERSITY OF MARYLAND
DEPT OF PHYSICS AND ASTRONOMY
ATTN H. R. GRIEM
COLLEGE PARK, MD 20742

MASSACHUSETTS INSTITUTE
OF TECHNOLOGY
PLASMA FUSION CENTER
ATTN G. BEKEFI
ATTN R. DAVIDSON
ATTN B. COPPI
ATTN R. J. HANSMAN, JR.
ATTN A. PALEVSKY
CAMBRIDGE, MA 02139

UNIVERSITY OF PENNSYLVANIA
MOORE SCHOOL
ATTN B. D. STEINBERG
PHILADELPHIA, PA 1910

POLYTECHNIC INSTITUTE OF NEW YORK
ATTN N. MARCUVITZ
ROUTE 110
FARMINGDALE, NY 11735

UNIVERSITY OF TENNESSEE
DEPT OF ELECTRICAL ENGINEERING
ATTN I. ALEXEFF
KNOXVILLE, TN 37916

UNIVERSITY OF WASHINGTON
DEPT OF PHYSICS
ATTN M. BAKER
SEATTLE, WA 98195

US ARMY ELECTRONICS RESEARCH
& DEVELOPMENT COMMAND
ATTN TECHNICAL DIRECTOR, DRDEL-CT
ATTN C. HARDIN, DRDEL-CT-EW

HARRY DIAMOND LABORATORIES
ATTN CO/TD/TSO/DIVISION DIRECTORS
ATTN RECORD COPY, 8120C
ATTN HDL LIBRARY, (3 COPIES) 81100
ATTN HDL LIBRARY, (WOODBRIDGE) 81100
ATTN TECHNICAL REPORTS BRANCH, 81300
ATTN CHAIRMAN, EDITORIAL COMMITTEE
ATTN CHIEF, 21000
ATTN CHIEF, 21100
ATTN CHIEF, 21200
ATTN CHIEF, 21300
ATTN CHIEF, 21400
ATTN CHIEF, 21500
ATTN CHIEF, 22000
ATTN CHIEF, 22100
ATTN CHIEF, 22300
ATTN CHIEF, 22800
ATTN CHIEF, 22900
ATTN CHIEF, 11000
ATTN CHIEF, 13000
ATTN CHIEF, 13200
ATTN CHIEF, 13300
ATTN CHIEF, 13500
ATTN GREYBILL, S., 22900
ATTN STEWART, A., 22900
ATTN KERRIS, K., 22900
ATTN WHITTAKER, D., 81300
ATTN ISLER, W., 13500
ATTN BROWN, E., 13500
ATTN WORTMAN, D., 13200
ATTN MCLEAN, F., 22800
ATTN BROMBORSKY, A., 22300 (20 COPIES)
ATTN KEHS, A., 22300 (20 COPIES)
ATTN GILBERT, R., 22300
ATTN VANDERWALL, J., 22300
ATTN CONWAY, T., 22300
ATTN BLACKBURN, J., 22300
ATTN MEYER, O., 22300
ATTN OLDHAM, T., 22300
ATTN MCLEAN, B., 22800
ATTN SILVERSTEIN, J., 13200
ATTN BRUNS, H., 21100 (20 COPIES)
ATTN HUTTLIN, G. A., 22900
ATTN SOLN, J., 22300
ATTN LEAVITT, R., 13200
ATTN CROWNE, F., 13200
ATTN MORRISON, C., 13200
ATTN GERLACH, H., 11100
ATTN BRANDT, H. E., 22300 (40 COPIES)